Journal of Molecular Liquids 382 (2023) 121847

Contents lists available at ScienceDirect

Journal of Molecular Liquids

journal homepage: www.elsevier.com/locate/molliq

# Clay-supported acidic ionic liquid as an efficient catalyst for conversion of carbohydrates to 5-hydroxymethylfurfural

Samahe Sadjadi [a,*], Neda Abedian-Dehaghani [b], Majid M. Heravi [b,*], Xuemin Zhong [c], Peng Yuan [d], Josep Duran [e], Albert Poater [e,*], Naeimeh Bahri-Laleh [f,*]

[a] Gas Conversion Department, Faculty of Petrochemicals, Iran polymer and Petrochemical Institute, PO Box 14975-112, Tehran, Iran
[b] Department of Chemistry, School of Physics and Chemistry, Alzahra University, PO Box 1993891176, Vanak, Tehran, Iran
[c] CAS Key Laboratory of Mineralogy and Metallogeny/Guangdong Provincial Key, Laboratory of Mineral Physics and Materials, Guangzhou Institute of Geochemistry, Chinese Academy of Sciences, Guangzhou 510640, China
[d] School of Environmental Science and Engineering, Guangdong University of Technology, Guangzhou 510006, China
[e] Institut de Química Computacional i Catàlisi and Departament de Química, Universitat de Girona, c/ Maria Aurèlia Capmany 69, 17003 Girona, Catalonia, Spain
[f] Polymerization Engineering Department, Iran Polymer and Petrochemical Institute (IPPI), P.O. Box 14965/115, Tehran, Iran

ARTICLE INFO

*Keywords:*
Halloysite
Catalyst
5-hydroxymethylfurfural
Ionic liquid
DFT
Biofuel

ABSTRACT

Halloysite nanoclay has been used as a natural support for the immobilization of an acidic ionic liquid with multiple acidic sites. To graft the ionic liquid on the halloysite, amino-functionalized halloysite was reacted with 2,4,6-trichloro-1,3,5-triazine and 2-aminopyrimidine successively to form heterocyclic ligand on halloysite, which was then converted to acidic ionic liquids through reaction with chlorosulfuric acid. The resultant catalyst was then characterized via SEM, EDS, and elemental mapping analysis, FTIR, XRD and TGA. Noteworthy, acid-base titration method confirmed that introduction of acidic ionic liquid significantly improved the Brønsted acidity of halloysite. The catalytic activity of the catalyst was investigated for conversion of various carbohydrates to 5-hydroxymethylfurfural. Gratifyingly, the results showed that the catalyst could promote the reaction of fructose, sucrose, glucose and galactose under mild reaction conditions (catalyst (0.03 g), at 85 °C in 70 min) to give the product in high to excellent yields. Computational DFT studies unveiled the reaction mechanism, pointing out the limiting steps kinetically, and in addition how important are the non-covalent interactions. Furthermore, the recycling tests confirmed high recyclability of the catalyst up to six runs.

## 1. Introduction

The depletion of fossil fuel resources and the increase in environmental issues consistent with the growing use of fossil fuels, such as global warming and pollution of ecosystems, as well as increase in energy demand threaten sustainable development [1]. As a solution to these challenges, biomass has been considered as a promising alternative for the conventional non-renewable energy resources [2]. In this pathway, carbohydrates have received immense attention and numerous studied have been devoted to find efficient routes for converting carbohydrates into value-added products, including biomass-based platform chemical compounds that can be applied for the production of biofuels [3]. According to the US department of Energy, one of the most important carbohydrate-derived platform compounds is 5-hydroxymethylfurfural (HMF) [4]. It can be applied for the production of a wide range of valuable chemicals, such as 2,5-dimethylfuran that is a potential biofuel, 5-hydroxy-4-keto-2-pentenoic acid that is employed for the synthesis of monomers for plastics, 2,5-bis(ethoxymethyl)furan and levulinic acid [5,6,7]. HMF can be produced by acid-catalyzed dehydration of hexoses [8], such as fructose, cellulose and glucose. Up to now, various homogeneous and heterogeneous acid catalysts have been reported, including heteropolyacids, Amberlyst-15 [9], acidic carbon materials, H-form zeolites [10], Lewis acids [11] and so on, to promote this reaction, among which acidic ionic liquids (ILs) [12] exhibited remarkable performance. ILs that are organic salts composed of organic cations and organic/inorganic anions can be devised in a way that possess acidic functional groups [13]. Actually, ionic liquids are attractive in a variety of applications, including solvents [14],

* Corresponding authors.
*E-mail addresses:* s.sadjadi@ippi.ac.ir (S. Sadjadi), mmheravi@alzahra.ac.ir (M.M. Heravi), albert.poater@udg.edu (A. Poater), n.bahri@ippi.ac.ir (N. Bahri-Laleh).

https://doi.org/10.1016/j.molliq.2023.121847
Received 10 February 2023; Received in revised form 1 April 2023; Accepted 12 April 2023
Available online 17 April 2023

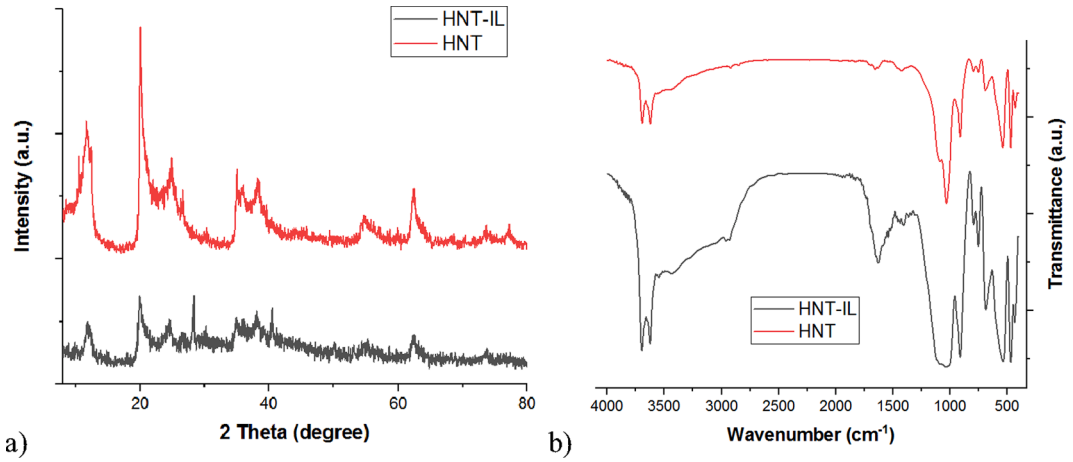


**Fig. 1.** (a) XRD patterns and (b) FTIR spectra of HNT and HNT-IL.

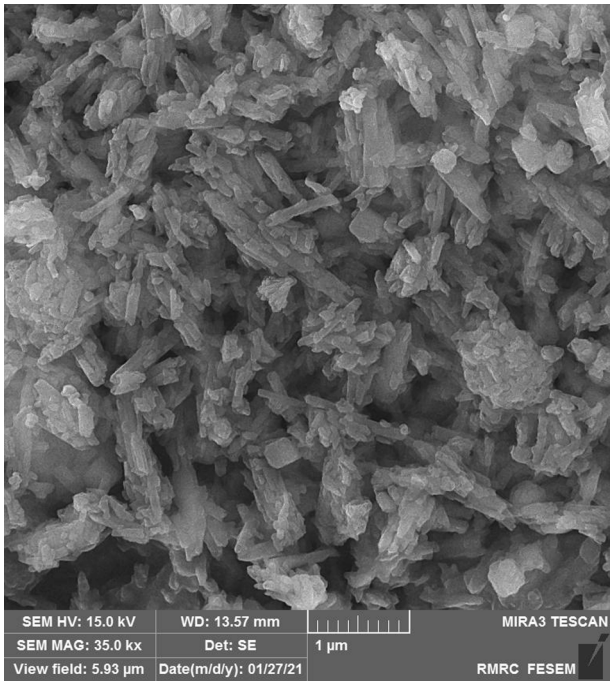


**Fig. 2.** SEM image of HNT-IL.

electrolytes [15] and catalysts [16,17]. In detail, ILs are useful in a bunch of chemical reactions including oxidation, reduction, and hydrolysis [16,18,19,20]. Actually, thanks to their unique properties, ILs can be used in reactions that are difficult to carry out using traditional catalysts. I addition, ILs can be easily supported on conventional supporting materials to furnish heterogeneous catalysts [21,22], which benefit from facile recovery, efficient recyclability and less environmental concerns [23]. In this regard, clays are considered as potential natural and low-cost supports to stabilize various catalytic species, including ILs. One class of clays that has received huge attention for catalytic purposes in recent years is halloysite (HNT) [24,25,26] that is a dioctahedral 1:1 clay mineral with tubular morphology [27,28] and general formula of ($Al_2(OH)_4Si_2O_5{\cdot}2H_2O$), and that could be considered a nanotube [29,30], with a bunch of applications, including support of metal catalysts [31,32,33] or as a material by itself [34,35]. Apart from high chemical, thermal and mechanical stability, large lumen (11–39%), the presence of hydroxyl groups on HNT surface and positively charged inner and negatively outer surfaces are other features of this clay. To date, our research group as well as dome others reported immobilization of conventional IL and polyionic liquids (PILs) on HNT to develop heterogeneous catalysts for various chemical reactions [36,37]. Motivated by excellent performance of HNT supported ILs [38,39], herein we wish to disclose a heterogeneous HNT-based acidic IL, which was prepared through covalent grafting of high loading of acidic IL on HNT. The catalytic activity, selectivity and recyclability of the catalyst, HNT-IL, for the dehydration of fructose to HMF were investigated and the effects of the reaction variables were appraised.

## 2. Experimental

### 2.1. Reagents

The acidic catalyst in this study was synthesized using the following reagents and solvents: HNT, 2,4,6-trichloro-1,3,5-triazine (TCT, 99%), 3-(aminopropyl)-triethoxysilane (APTES, 95%), chlorosulfuric acid (97%), 2-aminopyrimidine (97%), toluene (>99%), and tetrahydrofuran (THF, >99%). The substrates and solvents used to convert carbohydrates to HMF included, fructose (>99%), glucose (>99%), galactose (>99%), sucrose (>99%), cellulose, diethyl ether (>99%) and dimethyl sulfoxide (DMSO, >99%). All reagents and solvents mentioned were provided from Sigma-Aldrich and used as received.

### 2.2. Apparatus

This analysis was conducted with a Chemisorption Analyzer, NanoSORD (produced by Sensiran Co., Iran) with a heating ramp rate of 20 °C/min in a temperature range of 25–800 °C. To record the Fourier transform infrared (FT-IR) spectra of the catalyst and HNT, PERKIN-ELMER-Spectrum 65 device (scan time of 1 s and spectral resolution of 2 $cm^{-1}$, using KBr pellet) was applied. Thermogravimetric (TG) analysis of both HNT and the catalyst was performed using METTLER TOLEDO, under $O_2$ atmosphere and heating rate of 10 °C/min. X-ray diffraction (XRD) patterns of HNT and the catalyst were obtained via Siemens, D5000 equipped with Cu Kα radiation. Scanning electron microscopy (SEM) was carried out using VEGAII TESCAN scanning electron microscope, equipped with QX2, RONTEC energy dispersive X-ray analyzer. $^1$H Nuclear Magnetic Resonance ($^1$HNMR) spectroscopy was conducted with the Bruker DRX 400 MHz instrument in deuterated DMSO solvent to confirm formation of HMF. Gas chromatography–mass spectrometry (GC–MS) was also performed to identify HMF. Furthermore, Gas chromatography (GC) was applied, using an Agilent 6890 gas chromatograph with a flame ionization detector (FID) and G&W HP-5 ms GC column and nitrogen as a carrier gas at a split ratio of 100:1 to quantitatively determine HMF. The operating conditions of GC and

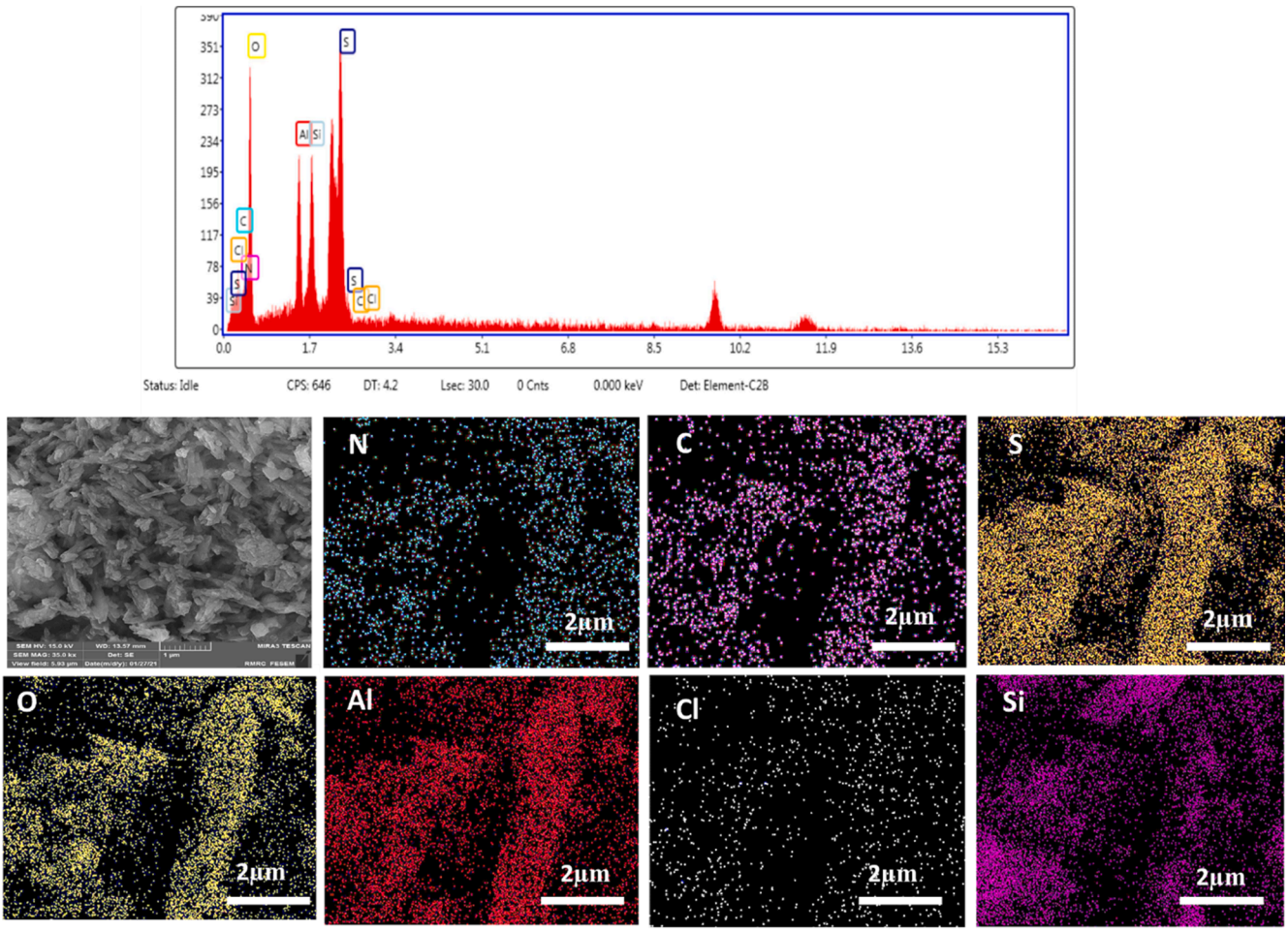


**Fig. 3.** EDS (above) and elemental mapping analysis (below) of HNT-IL.

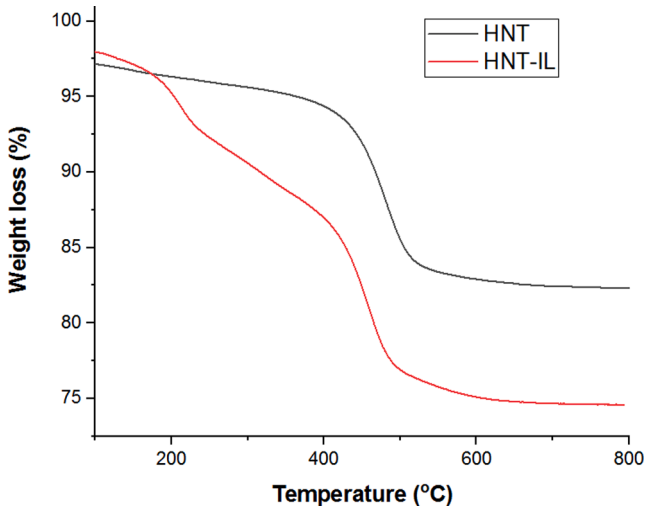


**Fig. 4.** TG thermograms of HNT and HNT-IL.

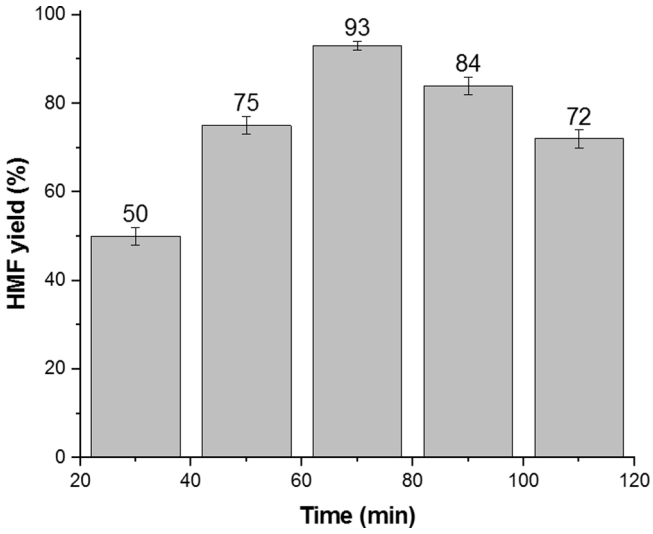


**Fig. 5.** Investigation of the effect of reaction time on the HMF yield. The reaction was performed using fructose (1 mmol) as substrate, HNT-IL (0.03 g) as catalyst and DMSO (5 mL) as solvent at 85 °C.

**Table 1**
The Brønsted acidity of the as-synthesized HNT-IL and HNT.

| | HNT-IL | HNT |
|---|---|---|
| NaOH (mL) | 38.85 | 1.0 |
| Acid loading (mmol.g$^{-1}$) | 7.77 | 0.2 |

GC–MS analyses were as follow: the inlet temperature was set at 275 °C and the detector temperature was set at 285 °C. The oven temperature was set at 60 °C for 1 min. Then the oven temperature increased to 280 °C at a rate of 20 °C.min$^{-1}$. The holding time at this temperature

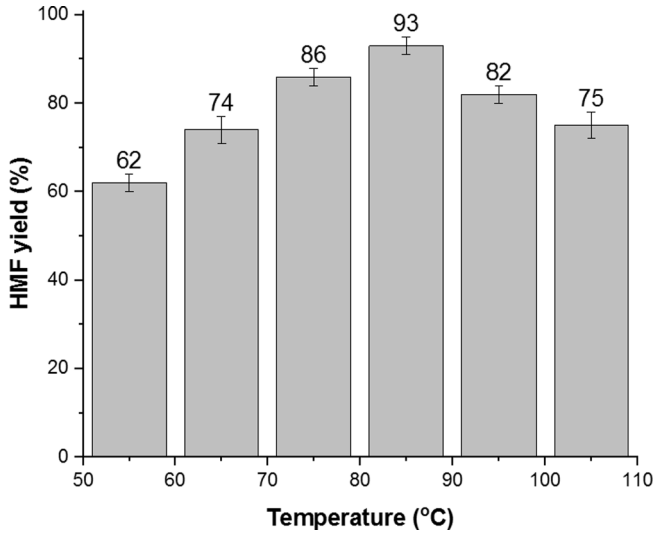


**Fig. 6.** Investigation of the effect of reaction temperature on the HMF yield. The reaction was performed using fructose (1 mmol) as substrate, HNT-IL (0.03 g) as catalyst and DMSO (5 mL) as solvent in 70 min.

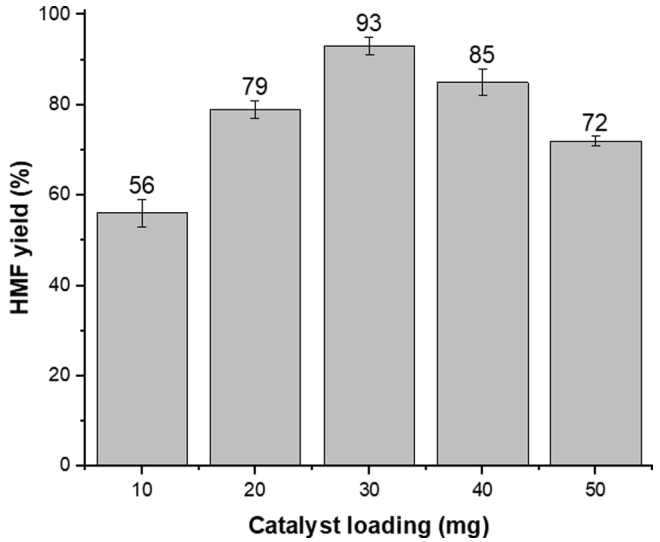


**Fig. 7.** Investigation of the effect of HNT-IL loading on the HMF yield. The reaction was performed using fructose (1 mmol) as substrate in DMSO (5 mL) as solvent at 85 °C.

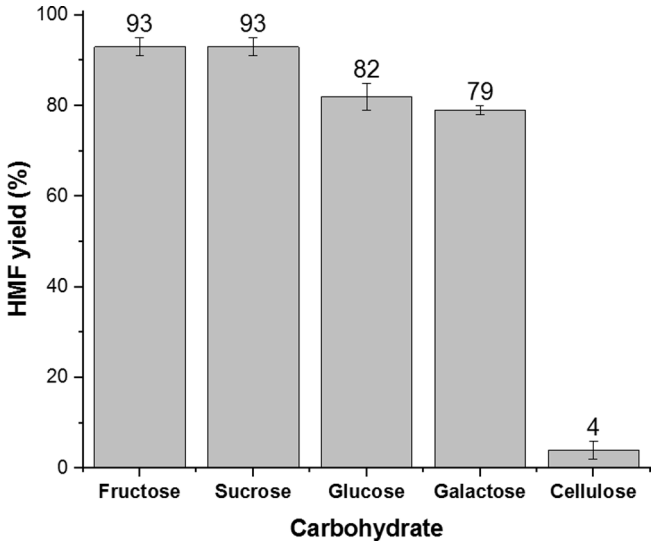


**Fig. 8.** The effect of the nature of carbohydrate on the HMF yield. Reaction conditions: carbohydrate (1 mmol), HNT-IL (0.03 g), DMSO (5 mL) at 85 °C in 70 min.

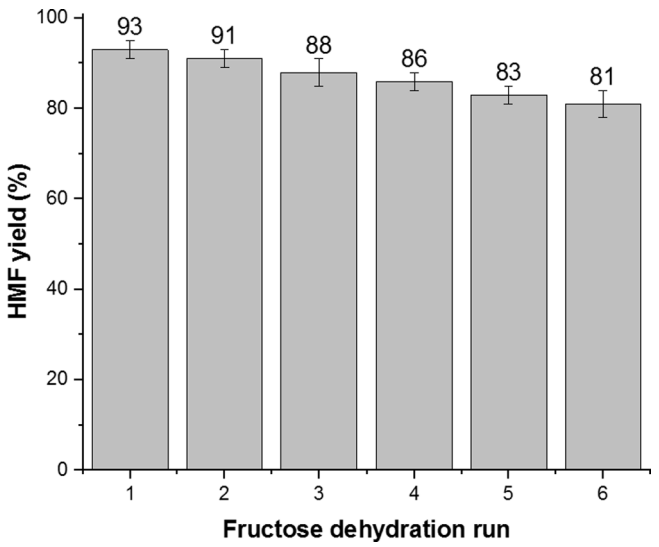


**Fig. 9.** Recyclability of HNT-IL for dehydration of fructose to HMF under the optimum reaction conditions.

was 5 and 12 min, respectively, for the run times of 17 and 24 min.

The products were characterized by high performance thin chromatography (HPLC). The used apparatus was Agilent 1200 Series, equipped with a Brisa LC2 C18 column (5 μm, 25 × 0.46) operated at 35 °C based on the external standard. The identities of the products were authenticated by comparing their retention times with those of pure compounds. An auto-sampler (Agilent G1329A) was utilized to enhance the reproducibility. HMF was quantified with an ultraviolet detector (Agilent G1365C MWD) at 282 nm. The eluent with flow rate of 1 mL $min^{-1}$ was a mixture of acetonitrile to water with volumetric ratio of 40:60.

### 2.3. Catalyst synthesis

Using our previous experiences on loading high content of IL on HNT [40], HNT was functionalized with an acidic IL and used as a metal-free catalyst to transform carbohydrates into HMF. To synthesize the catalyst, HNT was first amino-functionalized using APTES. For this purpose, HNT (2 g) was suspended in dry toluene and homogenized under ultrasonic irradiation (power 150 W, 20 min). APTES (1.5 mL) was then introduced and the mixture was refluxed overnight under Ar atmosphere. Subsequently, the resultant powder (HNT-N) was filtered, washed with dry toluene (3 * 20 mL) and dried in an oven at 60 °C overnight. In the next step, TCT was conjugated to HNT-N. In this line, TCT (4 mmol) was dissolved in THF (20 mL) and added to a stirred suspension of HNT-N (2 g) in THF (30 mL). The obtained mixture was then cooled to 0 °C for 24 h under stirring conditions. Afterwards, the solid (HNT-TCT) was separated, washed with THF several times and dried at 70 °C overnight. In the following, a solution of 2-aminopyrimidine (4 mmol) was prepared in THF (20 mL) and mixed with the suspension of HNT-TCT (2 g) in THF (30 mL). After refluxing for 24 h, the precipitate (HNT-T-P) was filtered, rinsed with THF for three times and dried at 70 °C overnight. Finally, to transform the heterocyclic moieties in IL, chlorosulfuric acid (10 mmol) was added to the suspension of HNT-T-P (2 g) in toluene and the obtained mixture was refluxed for 18 h.

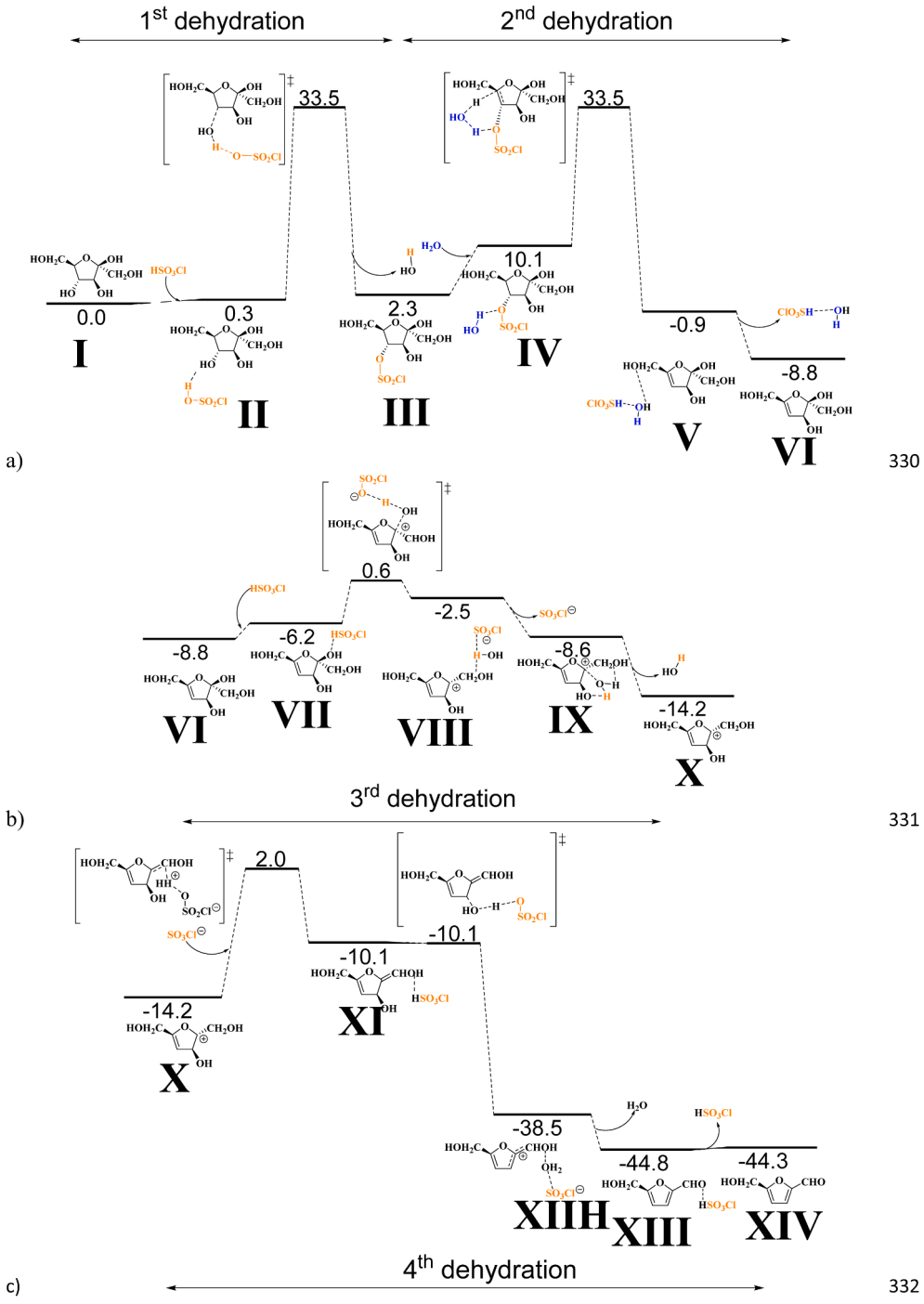


19

**Fig. 10.** Reaction pathway of the dehydration of fructose (I) to HMF (IV) splitted into the (a) first and second, (b) third and (c) fourth dehydrations, calculated at the B3LYP-D3/def2TZVP(smd-$H_2O$)//BP86-D3/Def2SVP level of theory (relative Gibbs energies in kcal/mol with respect to I).

Upon completion of the reaction, the solid (HNT-IL) was collected, washed with toluene three times and dried in an oven at 60 °C.

### 2.4. Transformation of carbohydrates to HMF

To transform carbohydrates into HMF, carbohydrates (100 mg) were dissolved in DMSO (10 mL) and stirred for 10 min at room temperature. Then, appropriate amount of HNT-IL (10–50 mg) was added and the mixture was stirred at a temperature range of 50–120 °C at different reaction times. The reaction mixture was then cooled and HNT-IL was collected by centrifugation. In order to recover the used catalyst, the separated HNT-IL was washed with DMSO repeatedly and then dried in an oven at 60 °C overnight. HMF purification was performed according to the previous report [41]. Briefly, water saturated with NaCl (10 mL) was added to the filtrate to separate the mixture into two phases, in which the organic layer (the upper phase) contains HMF and THF, while the aqueous layer (the lower phase) contains DMSO and small amount of HMF. The organic phase was then extracted using Rotary evaporation, and THF was separated. To extract the small amount of HMF in aqueous phase, diethyl ether (30 mL) was added to the aqueous phase. After the

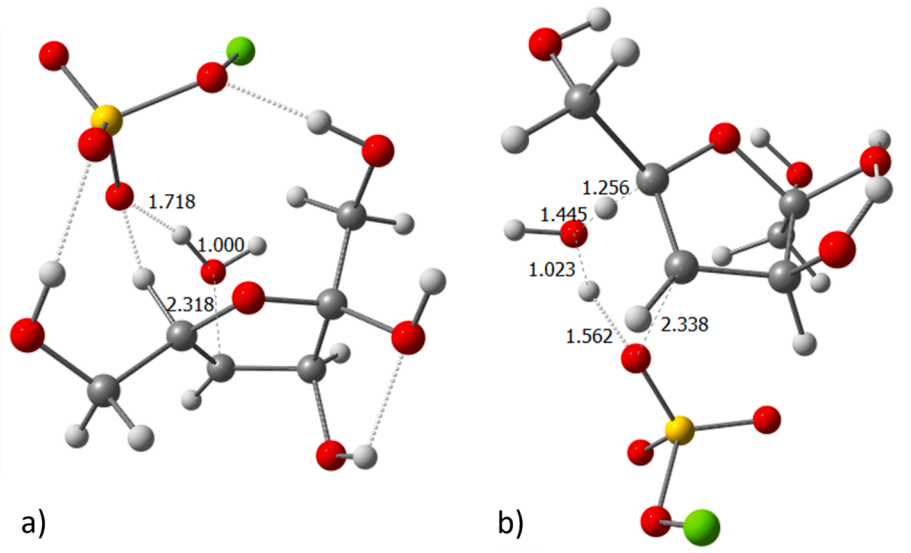


**Fig. 11.** Transition states (a) II-III and (b) IV-V; selected distances are in Å.

introduction of diethyl ether, two phases were formed, in which HMF was transferred to the organic phase (the upper phase) and then separated by distillation.

To obtain the reaction conversion Equation (1) was applied, where Mole (0) is the initial moles of carbohydrate and Mole (r) is the moles of remained carbohydrate.

$$Conversion(\%) = \frac{Mole(0) - Mole(r)}{Mole(0)} \times 100 \quad (1)$$

HMF yield can also be calculated via Equation (2).

$$HMFyield(\%) = \frac{Mole(HMF)}{Mole(0)} \times 100 \quad (2)$$

### 2.5. Computational details

Gaussian 16 package was applied to perform all the DFT calculations [42]. The geometry optimizations without symmetry constraints were performed using the pure GGA functional of Becke and Perdew, *i.e.* BP86 [43,44], together with the dispersion corrections to the energy through the Grimme D3 method [45], and the split-valence basis set (Def2SVP keyword in Gaussian) [46,47]. Apart from analytical frequency calculations to prove the nature of the stationary points, either minima or transition states, the Intrinsic Reaction Coordinate (IRC) procedure was used to confirm and extrapolate the two minima connected by each transition state. Furthermore, single point energy calculations using the hybrid GGA functional of Becke-Lee, Parr, and Yang, *i.e.* B3LYP [48,49,50], and the def2TZVP basis set for all atoms were performed [51]. In addition, any overestimation of the entropy was further explored with the model of Martin et al [52], with the applied version of Cavallo, Poater and coworkers [53,54,55], using 358.15 K as temperature and 1354 atm as pressure. Finally, the explicit effect of the solvent was included according to the polarizable solvation model (SMD), variation of IEFPCM of Truhlar and co-workers [56], applying water as a solvent. To sum up, the reported Gibbs energies in this work include energies obtained at the B3LYP-D3/def2TZVP(smd-H2O)//BP86-D3/Def2SVP level of theory corrected, with zero-point energies, thermal corrections and entropy effects evaluated with the BP86-D3/Def2SVP method.

## 3. Results and discussion

### 3.1. Characterization of HNT-IL

The structure and crystalline phase of the as-prepared HNT-IL were appraised by XRD. To elucidate whether the grafting of IL on HNT can lead to structural changes, the XRD pattern of HNT-IL was compared with that of HNT, Fig. 1a. The XRD pattern of HNT showed the peaks at $2\theta = 19.9, 24.4, 26.6, 38.5, 55.2, 62.5, 73.9$ and $77.4^{\circ}$, confirming that the used HNT for the synthesis of the catalyst had no impurities. The XRD pattern of HNT-IL, HNT peaks can be observed in lower intensity. This observation indicates grafting of IL. It is worth noting that preserve of HNT peaks with no displacement approves its stability during reactions for the grafting of IL on HNT.

In Fig. 1b, the comparison of FTIR spectra of HNT and HNT-IL is presented. The purchased HNT is of high purity and showed the bands at 3696 $cm^{-1}$ and 3625 $cm^{-1}$ (inner –OH), 1650 $cm^{-1}$ (weak stretching and bending vibrations of water molecules), 1101 $cm^{-1}$ (perpendicular Si-O-Si stretching), 1033 $cm^{-1}$ (Si-O stretching), 791 $cm^{-1}$ and 743 $cm^{-1}$ (symmetric stretching of Si-O and stretching vibration of Si-O respectively) and 535 $cm^{-1}$ (Al-O-Si vibration). All of these absorbance bands are detectable in the FTIR spectrum of HNT-IL, approving structural stability of HNT upon functionalization. Moreover, broadening of the absorbance band at 1608–1701 $cm^{-1}$ can be attributed to the –C=N functionality in IL moiety.

The morphological study of HNT-IL was carried out by recording its SEM images. As depicted in Fig. 2, in HNT-IL, the HNT tubes are recognizable, affirming that HNT preserved its morphology after functionalization with IL.

In Fig. 3, the results of EDS and elemental mapping analyses of HNT-IL are plotted. As expected, the EDS analysis detected Al, Si, O atoms that are the present atoms in HNT as well as C, N, S and Cl atoms that are indicative of IL moiety, confirming the grafting of IL into HNT. Regarding elemental mapping analysis, the high dispersion of the atoms in IL, *i.e.* C, N, O, S and Cl approves that IL was conjugated to HNT homogeneously.

TG is a powerful analysis that can not only shows the thermal stability of HNT-IL, but also confirms conjugation of IL onto HNT support. Comparison of the TG curves of HNT and HNT-IL in Fig. 4 indicates that the two thermograms are significantly distinguishable. In more detail, HNT as a clay mineral exhibited high thermal stability and only loss of structural water, and dehydroxylation (490 °C) were detected in the HNT thermogram that is in good agreement with the literature [57]. In

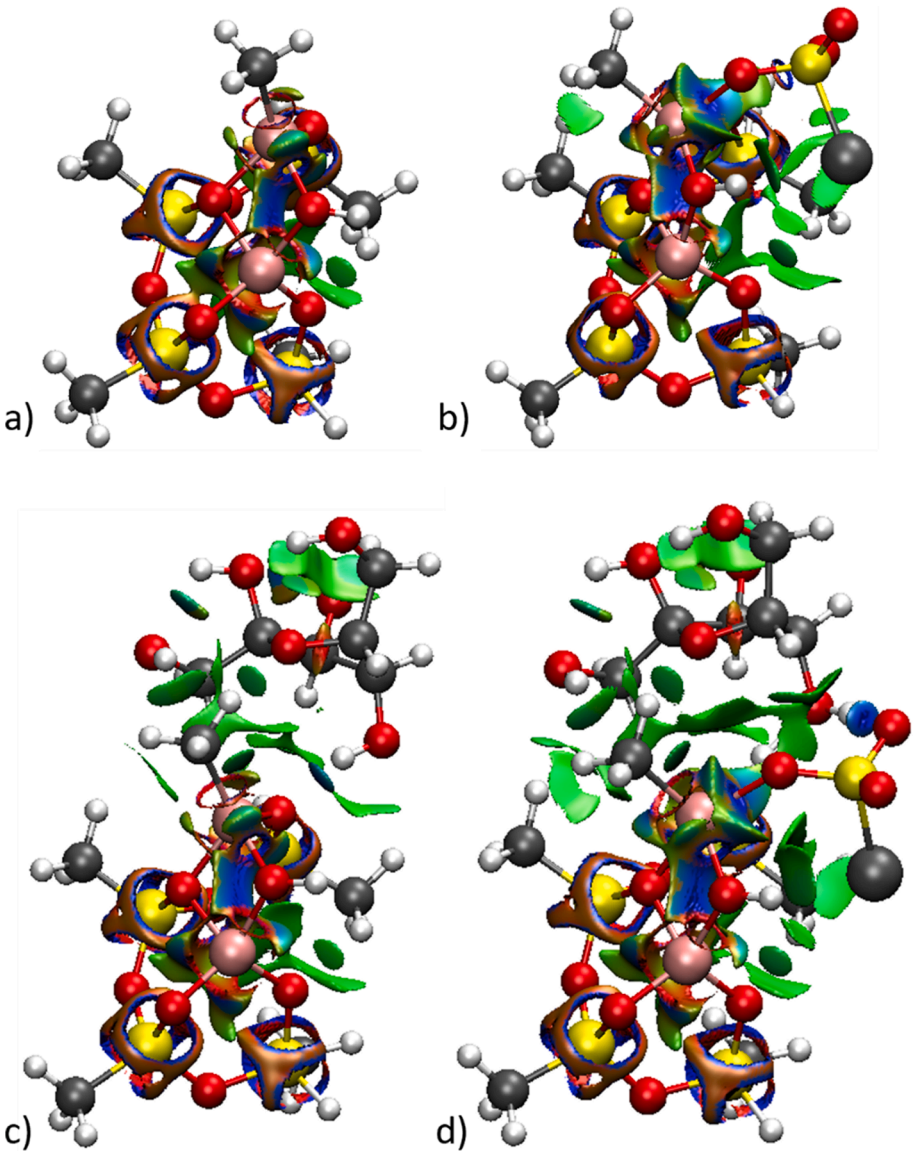


**Fig. 12.** NCI plots of the (a) halloysite model, (b) together with either $HSO_3Cl$ or (c) the substrate, and (d) both (C = gray; H = white; Si = yellow; Al = light red; Cl = dark gray). (For interpretation of the references to color in this figure legend, the reader is referred to the web version of this article.)

the case of HNT-IL, the main difference is the appearance of a new weight loss at 245 °C (about 30 wt%), which is indicative of the degradation of the IL moiety.

As mentioned earlier, the acidity of the catalyst is a crucial factor for the fructose dehydration to HMF. Hence, in the catalyst design an attempt was made to introduce an organic moiety with several acidic IL sites. To evaluate whether the acidic IL moiety increased the acidity, the Brønsted acidity of HNT and HNT-IL was estimated via acid-base titration method. According to the results, Table 1, introduction of acidic IL on HNT highly affected its Brønsted acidity and HNT-IL was almost eight time more acidic than HNT.

### 3.2. Catalytic activity of HNT-IL for dehydration of fructose

Considering the importance of HMF as an intermediate for the production of biofuels, the catalytic activity of HNT-IL for the dehydration of fructose to HMF was investigated. This reaction is an acid-catalyzed reaction that can be performed in the liquid phase and the main reaction variables in this chemical transformation are reaction time, temperature and catalyst loading. Hence, optimization of these parameters was conducted to achieve the highest reaction conversion and HMF yield.

### 3.3. Effect of reaction time on dehydration of fructose

To appraise the effect of reaction time, the dehydration of fructose was carried out at 85 °C using 0.03 g HNT-IL as the catalyst, and HMF yield was monitored at intervals of short time. The results in Fig. 5 implied that by increasing the reaction time from 30 to 70 min, HMF yield enhanced from 50 to 93%. However, a further increase in the reaction time had a detrimental effect on the HMF yield, and actually, the HMF yield decreased to 72 % after 110 min. According to the literature, this observation can be attributed to the degradation of HMF and the occurrence of side reactions [58]. Moreover, the formation of humins from condensation of HMF can potentially cover the active sites of HNT-IL and account for the decrease in HMF yield by prolonging the reaction [59].

### 3.4. Effect of reaction temperature on the dehydration of fructose

Next, the effect of reaction temperature was studied by repeating fructose dehydration at different temperatures, ranging from 55 to

105 °C. According to the results in Fig. 6, increase of reaction temperature from 55 to 85 °C resulted in improvement of HMF yield from 62 to 93%. Notably, 85 °C was the optimum value for reaction temperature and further increase of this parameter led to the decrease of HMF yield and change of the color of the reaction mixture from bright yellow to brown. This finding can also be rationalized by considering the possibility of formation of soluble polymers and humins from HMF condensation at elevated temperatures.

### 3.5. Effect of HNT-IL loading on dehydration of fructose

Another effective parameter on the HMF yield is the HNT-IL loading. To evaluate the effect of this parameter, dehydration of fructose was conducted in the presence of various loadings of HNT-IL (10–50 mg) and the obtained HMF yield for each run was compared in Fig. 7. As displayed, increasing HNT-IL from 10 to 30 mg resulted in an increase of HMF yield from 56 to 93 %. In fact, by increasing the catalyst loading, the number of the active sites increased and consequently the HMF yield enhanced. However, the results indicated that by increasing the HNT-IL loading from 30 to 50 mg, a reverse effect was observed and the HMF yield decreased. This issue supports the important role of catalyst loading in the HMF yield. More accurately, when the catalyst loading higher than the optimum value is used, numerous acidic sites of HNT-IL induce the HMF condensation and the humins formation, which is detrimental to the HMF yield.

### 3.6. Effect of the nature of carbohydrate

As described, HNT-IL showed excellent catalytic activity and selectivity for the dehydration of fructose to HMF. To elucidate whether this catalyst can promote the reaction of other carbohydrates to furnish HMF, the dehydration reaction for various carbohydrates, including glucose, galactose, sucrose and cellulose was carried out under the optimum reaction conditions, Fig. 8. Considering the mechanism of dehydration of carbohydrates to HMF, it is believed that in the case of sucrose that is composed of glucose and fructose units, the reactions involved hydrolysis, isomerization of glucose to fructose and dehydration to HMF. As displayed in Fig. 8, HNT-IL could successfully promote this reaction to furnish HMF with a similar yield compared to fructose. In the case of using glucose and galactose, slightly lower HMF yields (82 and 79%, respectively) were obtained. These results further confirm the high efficiency of HNT-IL for the transformation of carbohydrates to HMF. Notably, use of cellulose that consists of glucose units as a starting material led to a poor yield of HMF, indicating that the nature of the carbohydrate can affect the reaction conversion and HMF yield.

### 3.7. Recovery and recyclability of HNT-IL

Considering the importance of HMF synthesis from an industrial point of view, the development of highly efficient and low-cost catalysts with high activity, HMF selectivity and recyclability is of a high priority. Gratifyingly, HNT-IL that is a bio-based metal-free catalyst exhibited high activity and selectivity towards HMF. However, since the facile recovery and high recyclability of a heterogeneous catalyst is a determining factor for its large-scale uses, the study of recyclability of HNT-IL is imperative. In this line, HNT-IL recovered from dehydration of fructose (see Experimental section) was reused for the next reaction run under similar conditions. This recovery-reuse cycle was repeated for six reaction runs and the reaction conversion and HMF yield were measured after each run. As depicted in Fig. 9, HNT-IL exhibited high recyclability and only insignificant loss of the catalytic activity was detected after each run of the reaction. This issue can be attributed to the covalent conjugation of the acidic IL on HNT that ruled out the possibility of IL leaching from the HNT. The decrement of the catalytic activity can be ascribed to the coverage of the active sites of the catalyst by the organic products.

### 3.8. Molecular modeling results

In order to be able to determine precisely how the reaction of fructose, species **I**, with $HSO_3Cl$ takes place, calculations were carried out with the Density Functional Theory (DFT) method. Step by step, in Fig. 10a the mechanism starts from the fact that the interaction of both reactants is thermodynamically not disfavored, representing only an insignificant cost of 0.3 kcal/mol. From adduct **II**, $HSO_3Cl$ facilitates the dehydration of a hydroxyl group, providing it with a proton. This transition state step (TS) **II-III** kinetically requires 33.2 kcal/mol (see Fig. 11a). Then a water is symbolically added, which can be the same released in the previous step, with a key importance in the form of assistance in the TS **IV-V** to get a proton removed from the 5-membered ring of sucrose, specifically the one that is in alpha, preferably the one that contains $CH_2OH$ and not OH due to its greater Brønsted acidity. In this step the additional $H_2O$ gives a proton to the $SO_3Cl$ anionic unit attached to the 5-membered ring and at the same time the hydroxyl is the proton withdrawing agent. In fact, this role of the hydroxyl could be played differently by the $SO_3Cl$ anion, but a water facilitates passage with a 6-membered ring, instead of a highly strained 4-membered one. Either way, it describes a remarkable energy barrier of 23.4 kcal/mol, and not only, since if this is referenced with the previous intermediate of lowest energy, that is, **I**, where we would have the 2 reactants separately, we arrive at an energy barrier of 33.5 kcal/mol, which it shares with the previous **I-II** of being both the rate determining state (rds) [60,61]. To further verify that the correction for the overestimation of the entropy was not responsible for this tie, they were redone without the approximation of Martin and collaborators [52], and likewise the energy barriers coincided, obviously since between the two transition states there is no difference in chemical composition [62].

After the first two dehydrations, Fig. 10b starts with the second participation of reagent $HSO_3Cl$, not necessarily from the beginning, but obtained reaching intermediate **VI**. It allows the protonation of the hydroxyl that remains in alpha to the oxygen of the 5-membered ring, overcoming the TS **VII-VIII** with a reasonable energy barrier of 6.8 kcal/mol, and the system in addition to this slightly unfavorable kinetics also enjoys a high thermodynamic stabilization losing the $SO_3Cl^-$ anion and a water molecule, until reaching the cationic intermediate **X**, 14.2 kcal/mol below **I**. Then, according to the results in Fig. 10c, there is no need to enter into a debate as to whether the total dissociation of the previous anion $SO_3Cl^-$ is feasible because in the TS **X-XI**, with a barrier of 16.2 kcal/mol, it must return to participate as a base to remove a hydrogen from the methylene group, facilitating the process thanks to the carbocationic character. Then with a barrierless step, the remaining hydroxyl of the 5-membered ring undergoes a third step of dehydration with $HSO_3Cl$, thus reaching an intermediate **XIII** 44.8 kcal/mol more stable than **I**, but where the anionic moiety $SO_3Cl^-$ already has taken the proton from the carbocationic hydroxyl of the previous intermediate **XII**, without any possibility of calculating its transition state when the fourth dehydrative step takes effect. Finally, product **XIV** is almost isoenergetic, simply excluding a molecule of $HSO_3Cl$. Thus, looking back at all the steps in Fig. 10, it is clear that $HSO_3Cl$, in addition to acting as a reagent, also acts autocatalytically, at certain times. Even though the halloysite moiety was excluded to unveil the right reaction mechanism without conformational problems that would be unreal considering the high flexibility of the halloysite, to stress the importance of the interaction with $HSO_3Cl$ was incorporated to find the binding energy. If we considered the halloysite in the calculations it is clear that $HSO_3Cl$ also plays a fundamental role with a strong interaction with the halloysite, leading to a thermodynamic stabilization over 10.7 kcal/mol, with a Al···O interaction, close to a real bond, since the Mayer Bond Order (MBO) was 0.484, to be compared with the MBOs of the Al-O bonds that are not lower than 0.720, except for the Au-O bond trans to the entering $HSO_3Cl$ that is 0.558 [24,26,63]. In addition, according to the NCIplots by Contreras et al. [64,65], the halloysite creates a large number of H-bonds with both the substrate and the $HSO_3Cl$, but specially the latter,

and actually, the energy stabilization is more due to the $HSO_3Cl$ than the substrate, since the interaction with the substrate is unfavorable by 8.3 kcal/mol, whereas combined with $HSO_3Cl$ leads to a favorable interaction of 12.1 kcal/mol. Fig. 12 shows the attractive interactions, including also more stabilized blue interactions for those O···H interactions. The non covalent interactions are clear between the hydrogen and oxygen atoms of the halloysite and also the substrate, and vice versa. However, the strongest ones are due to the H-bonds between the chloride and the hydrogen atoms of the halloysite.

## 4. Conclusions

A new Halloysite supported catalyst, HNT-IL, beneficing acidic ionic liquid type ligands was successfully synthesized and employed in the dehydration of common carbohydrates to furnish 5-hydroxymethylfurfural (HMF), known as an efficient intermediate for 2,5-dimethylfuran (potential biofuel) production [66,67]. In this regard, first effect of reaction parameters of fructose dehydration reaction on reaction conversion and HMF yield was surveyed thoroughly. According to the conducted experiments, a reaction time (70 min), reaction temperature (83 °C), catalyst dosage (30 mg), were obtained as optimum amounts in which both reaction conversion and HMF yield reached outstandingly high value of 98 %. The designed catalyst could outstandingly promote the fructose dehydrogenation up to 5 consecutive runs with insignificant depression in HMF yield. Then, DFT calculations shed light to understand the mechanism and why a temperature of 356.15 K is needed at the experimental level. Due to the complexity, not due to the size of the fructose, but due to the high volume of H-bond interactions, halloysite was omitted in the DFT calculations, but it is a point to consider for future studies, especially because it could hinder the action of $HSO_3Cl$ and/or water as a catalyst in certain cases; but also blocking the potential formation of minority products other than the HMF.

### *CRediT authorship contribution statement*

**Samahe Sadjadi:** Supervision, Conceptualization. **Neda Abedian-Dehaghani:** Investigation. **Majid M. Heravi:** Supervision, Conceptualization. **Xuemin Zhong:** Investigation. **Peng Yuan:** Supervision, Conceptualization. **Josep Duran:** Investigation. **Albert Poater:** Supervision, Conceptualization. **Naeimeh Bahri-Laleh:** Supervision, Conceptualization.

### Declaration of Competing Interest

The authors declare that they have no known competing financial interests or personal relationships that could have appeared to influence the work reported in this paper.

### Data availability

The data is included in the SI, and further detail can be requested to the authors.

### Acknowledgments

This research has been supported by the National Natural Science Foundation of China (Grant Nos. 52161145405 and 41972045), Iran National Science Foundation (INSF) under project No. 4000580. The authors also appreciate the partial supports of Iran Polymer and Petrochemical Institute and Al-zahra University. A.P. is grateful for financial support from the Ministerio de Ciencia e Innovación (PID2021-127423NB-I00) and the Generalitat de Catalunya (project 2021 SGR0623) and ICREA Academia prize 2019. A.P. is a Serra Húnter fellow. We thank the support from BSC supercomputing facilities.

## Appendix A. Supplementary material

Supplementary data to this article can be found online at https://doi.org/10.1016/j.molliq.2023.121847.

## References

[1] Q. Hou, M. Zhen, L. Liu, Y. Chen, F. Huang, S. Zhang, W. Li, M. Ju, Tin phosphate as a heterogeneous catalyst for efficient dehydration of glucose into 5-hydroxymethylfurfural in ionic liquid, Appl. Catal. B 224 (2018) 183–193.
[2] F.F. Costa, D. Terra de Oliveira, Y. Pereira Brito, G.N. da Rocha Filho, C. F. Alvarado, A.M. Balu, R. Luque, L.A. Santos do Nascimento,, Lignocellulosics to biofuels: an overview of recent and relevant advances, Curr. Opin. Green Sustain. Chem. 24 (2020) 21–25.
[3] Y. Ma, S. Qing, L. Wang, N. Islam, S. Guan, Z. Gao, X. Mamat, H. Li, W. Eli, T. Wang, Production of 5-hydroxymethylfurfural from fructose by a thermo-regulated and recyclable Brønsted acidic ionic liquid catalyst, RSC Adv. 5 (2015) 47377–47383.
[4] F. Guo, Z. Fang, T.-J. Zhou, Conversion of fructose and glucose into 5-hydroxymethylfurfural with lignin-derived carbonaceous catalyst under microwave irradiation in dimethyl sulfoxide–ionic liquid mixtures, Bioresour. Technol. 112 (2012) 313–318.
[5] H. Li, Q. Zhang, X. Liu, F. Chang, Y. Zhang, W. Xue, S. Yang, Immobilizing $Cr^{3+}$ with $SO_3H$-functionalized solid polymeric ionic liquids as efficient and reusable catalysts for selective transformation of carbohydrates into 5-hydroxymethylfurfural, Bioresour. Technol. 144 (2013) 21–27.
[6] M. Cardona-Farreny, P. Lecante, J. Esvan, C. Dinoi, I. Del Rosal, K. Philippot, M. R. Axet, Bimetallic RuNi nanoparticles as catalysts for upgrading biomass: metal dilution and solvent effects on selectivity shifts, Green Chem. 23 (2021) 8480–8500.
[7] L. Bruna, M. Cardona-Farreny, V. Colliere, K. Philippot, M.R. Axet, In situ ruthenium catalyst modification for the conversion of furfural to 1,2-pentanediol, Nanomaterials 12 (2022) 328.
[8] K.I. Galkin, V.P. Ananikov, When will 5-hydroxymethylfurfural, the "sleeping giant" of sustainable chemistry, Awaken? ChemSusChem 12 (2019) 2976–2982.
[9] F.H. Richter, K. Pupovac, R. Palkovits, F. Schüth, Set of acidic resin catalysts to correlate structure and reactivity in fructose conversion to 5-hydroxymethylfurfural, ACS Catal. 3 (2013) 123–127.
[10] A. Pande, P. Niphadkar, K. Pandare, V. Bokade, Acid modified H-USY zeolite for efficient catalytic transformation of fructose to 5-hydroxymethyl furfural (biofuel precursor) in methyl isobutyl ketone-water biphasic system, Energy Fuels 32 (2018) 3783–3791.
[11] T. Deng, X. Cui, Y. Qi, Y. Wang, X. Hou, Y. Zhu, Conversion of carbohydrates into 5-hydroxymethylfurfural catalyzed by $ZnCl_2$ in water, Chem. Commun. 48 (2012) 5494–5496.
[12] P.V. Rathod, R.B. Mujmule, W.-J. Chung, A.R. Jadhav, H. Kim, Efficient dehydration of glucose, sucrose, and fructose to 5-hydroxymethylfurfural using tricationic ionic liquids, Catal. Lett. 149 (2019) 672–687.
[13] F. Tao, H. Song, L. Chou, Dehydration of fructose into 5-hydroxymethylfurfural in acidic ionic liquids, RSC Adv. 1 (2011) 672–676.
[14] V. Hessel, N.N. Tran, M.R. Asrami, Q.D. Tran, N. Van Duc Long, M. Escribà-Gelonch, J.O. Tejada, S. Linke, K. Sundmacher, Sustainability of green solvents-review and perspective, Green Chem. 24 (2022) 410–437.
[15] X. Tan, X. Sun, B. Han, Ionic liquid-based electrolytes for $CO_2$ electroreduction and $CO_2$ electroorganic transformation. Nat. Sci. Rev. 9 (2022) nwab022.
[16] Y. Yamazaki, M. Miyaji, O. Ishitani, Utilization of low-concentration $CO_2$ with molecular catalysts assisted by $CO_2$-capturing ability of catalysts, additives, or reaction media, J. Am. Chem. Soc. 144 (2022) 6640–6660.
[17] V.I. Pârvulescu, C. Hardacre, Catalysis in ionic liquids, Chem. Rev. 107 (2007) 2615–2665.
[18] P. Wasserscheid, W. Keim, Ionic liquids - New 'solutions' for transition metal catalysis, Angew. Chem. Int. Ed. 39 (2000) 3772–3789.
[19] A.R. Shaikh, S. Posada-Pérez, A. Brotons-Rufes, J.J. Pajski, G. Vajiha, A. Kumar, A. Mateen, M. Poater, M. Solà, L.C. Chawla, Selective absorption of $H_2S$ and $CO_2$ by azole based protic ionic liquids: a combined density functional theory and molecular dynamics study, J. Mol. Liq. 367 (2022), 120558.
[20] A.R. Shaikh, M. Ashraf, T. AlMayef, M. Chawla, A. Poater, L. Cavallo, Amino acid ionic liquids as potential candidates for $CO_2$ capture: Combined density functional theory and molecular dynamics simulations, Chem. Phys. Lett. 745 (2020), 137239.
[21] G. Kaur, H. Kumar, M. Singla, Diverse applications of ionic liquids: a comprehensive review, J. Mol. Liq. 351 (2022), 118556.
[22] T.M. Dhameliya, P.R. Nagar, K.A. Bhakhar, H.R. Jivani, B.J. Shah, K.M. Patel, V. S. Patel, A.H. Soni, L.P. Joshi, N.D. Gajjar, Recent advancements in applications of ionic liquids in synthetic construction of heterocyclic scaffolds: a spotlight, J. Mol. Liq. 348 (2022), 118329.
[23] B. Karimi, B. Ghaffari, H. Vali, Synergistic catalysis within core-shell $Fe_3O_4$@$SiO_2$ functionalized with triethylene glycol (TEG)-imidazolium ionic liquid and tetramethylpiperidine N-oxyl (TEMPO) boosting selective aerobic oxidation of alcohols, J. Colloid Interface Sci. 589 (2021) 474–485.
[24] S. Shams, S. Sadjadi, J. Duran, S. Simon, A. Poater, N. Bahri-Laleh, Effect of support hydrophobicity of halloysite based catalysts on the PAO hydrofinishing performance, Appl. Organomet. Chem. 36 (2022) e6719.

[25] S. Karimi, N. Bahri-Laleh, S. Sadjadi, G. Pareras, A.P. Nekoomanesh-Haghighi, Pd on nitrogen rich polymer-halloysite nanocomposite as an environmentally benign and sustainable catalyst for hydrogenation of polyalfaolefin based lubricants, J. Ind. Eng. Chem. 97 (2021) 441–451.
[26] S. Dehghani, S. Sadjadi, N. Bahri-Laleh, M. Nekoomanesh-Haghighi, M., Poater, A., Study of the effect of the ligand structure on the catalytic activity of Pd@ ligand decorated halloysite: combination of experimental and computational studies, Appl. Organomet. Chem. 33 (2019) e4891.
[27] V.A. Vinokurov, A.V. Stavitskaya, E.V. Ivanov, P.A. Gushchin, D.V. Kozlov, A. Y. Kurenkova, P.A. Kolinko, E.A. Kozlova, Y.M. Lvov, Halloysite nanoclay based CdS formulations with high catalytic activity in hydrogen evolution reaction under visible light irradiation, ACS Sustainable Chem. Eng. 5 (2017) 11316–11323.
[28] L. Deng, Effects of calcination and acid treatment on improving benzene adsorption performance of halloysite, Appl. Clay Sci. 181 (2019), 105240.
[29] G. Lazzara, G. Cavallaro, A. Panchal, R.F. Fakhrullin, An assembly of organic-inorganic composites using halloysite clay nanotubes, Curr. Opin. Colloid Interface Sci. 35 (2018) 42–50.
[30] G. Cavallaro, L. Chiappisi, P. Pasbakhsh, M. Gradzielski, G. Lazzara, A structural comparison of halloysite nanotubes of different origin by Small-Angle Neutron Scattering (SANS) and electric birefringence, Appl. Clay Sci. 160 (2018) 71–80.
[31] V. Vinokurov, A. Stavitskaya, A. Glotov, A. Ostudin, M. Sosna, P. Gushchin, Y. Darrat, Y. Lvov, Halloysite nanotube-based cobalt mesocatalysts for hydrogen production from sodium borohydride, J. Solid State Chem. 268 (2018) 182–189.
[32] H. Wang, D. Wu, X. Li, P. Huo, Ce doping $TiO_2$/halloysite nanotubes photocatalyst for enhanced electrons transfer and photocatalytic degradation of Tetracycline, J. Mater. Sci.: Mater. Electron. 30 (2019) 19126–19136.
[33] M. Mehdizadeh, S. Sadjadi, A. Poater, A. Mansouri, N. Bahri-Laleh, Molecular modelling aided catalyst design for PAO oils hydrofinishing, J. Mol. Liq. 352 (2022), 118675.
[34] T. Yu, L.T. Swientoniewski, M. Omarova, M.-C. Li, I.I. Negulescu, N. Jiang, O. A. Darvish, A. Panchal, D.A. Blake, Q. Wu, Y.M. Lvov, V.T. John, D. Zhang, Investigation of amphiphilic polypeptoid-functionalized halloysite nanotubes as emulsion stabilizer for oil spill remediation, ACS Appl. Mater. Interfaces 11 (2019) 27944–27953.
[35] R.J. Smith, K.M. Holder, S. Ruiz, W. Hahn, Y. Song, Y.M. Lvov, J.C. Grunlan, Environmentally benign halloysite nanotube multilayer assembly significantly reduces polyurethane flammability, Adv. Funct. Mater. 28 (2018) 1703289.
[36] S. Sadjadi, Halloysite-based hybrids/composites in catalysis, Appl. Clay Sci. 189 (2020), 105537.
[37] S. Sadjadi, F. Koohestani, G. Pareras, M. Nekoomanesh-Haghighi, N. Bahri-Laleh, A. Poater, Combined experimental and computational study on the role of ionic liquid containing ligand in the catalytic performance of halloysite-based hydrogenation catalyst, J. Mol. Liq. 331 (2021), 115740.
[38] K.B. Shishkhanova, V.S. Molchanov, A.N. Baranov, E.P. Kharitonova, A.S. Orekhov, N.A. Arkharova, O.E. Philippova, A pH-triggered reinforcement of transient network of wormlike micelles by halloysite nanotubes of different charge, J. Mol. Liq. 370 (2023), 121032.
[39] S. Yousefi, N. Bahri-Laleh, M. Nekoomanesh, M. Emami, S. Sadjadi, S. A. Mirmohammadi, M. Tomasini, E. Bardají, A. Poater, An efficient initiator system containing $AlCl_3$ and supported ionic-liquid for the synthesis of conventional grade polyisobutylene in mild conditions, J. Mol. Liq. 367 (2022), 120381.
[40] S. Sadjadi, F. Koohestani, N. Abedian-Dehaghani, M.M. Heravi, Halloysite nanoclay with high content of sulfonic acid-based ionic liquid: a novel catalyst for the synthesis of tetrahydrobenzob]pyrans, Catalysts 11 (2021) 1172.
[41] J. Wang, J. Ren, X. Liu, G. Lu, Y. Wang, High yield production and purification of 5-hydroxymethylfurfural, AIChE J. 59 (2013) 2558–2566.
[42] Gaussian 16, Revision C.01, M.J. Frisch, G.W. Trucks, H.B. Schlegel, G.E. Scuseria, M.A. Robb, J.R. Cheeseman, G. Scalmani, V. Barone, G.A. Petersson, H. Nakatsuji, X. Li, M. Caricato, A.V. Marenich, J. Bloino, B.G. Janesko, R. Gomperts, B. Mennucci, H.P. Hratchian, J.V. Ortiz, A.F. Izmaylov, J.L. Sonnenberg, D. Williams-Young, F. Ding, F. Lipparini, F. Egidi, J. Goings, B. Peng, A. Petrone, T. Henderson, D. Ranasinghe, V.G. Zakrzewski, J. Gao, N. Rega, G. Zheng, W. Liang, M. Hada, M. Ehara, K. Toyota, R. Fukuda, J. Hasegawa, M. Ishida, T. Nakajima, Y. Honda, O. Kitao, H. Nakai, T. Vreven, K. Throssell, J.A. Montgomery, Jr., J.E. Peralta, F. Ogliaro, M.J. Bearpark, J.J. Heyd, E.N. Brothers, K.N. Kudin, V.N. Staroverov, T.A. Keith, R. Kobayashi, J. Normand, K. Raghavachari, A.P. Rendell, J.C. Burant, S.S. Iyengar, J. Tomasi, M. Cossi, J.M. Millam, M. Klene, C. Adamo, R. Cammi, J.W. Ochterski, R.L. Martin, K. Morokuma, O. Farkas, J.B. Foresman, D.J. Fox, Gaussian, Inc., Wallingford CT, 2016.
[43] A.D. Becke, Density-functional exchange-energy approximation with correct asymptotic behavior, Phys. Rev. A 38 (1988) 3098–3100.
[44] J.P. Perdew, Density-functional approximation for the correlation energy of the inhomogeneous electron gas, Phys. Rev. B 33 (1986) 8822–8824.
[45] S. Grimme, J. Antony, S. Ehrlich, H. Krieg, A consistent and accurate ab initio parametrization of density functional dispersion correction (DFT-D) for the 94 elements H-Pu, J. Chem. Phys. 132 (2010), 154104.
[46] F. Weigend, R. Ahlrichs, Balanced basis sets of split valence, triple zeta valence and quadruple zeta valence quality for H to Rn: design and assessment of accuracy, Phys. Chem. Chem. Phys. 7 (2005) 3297–3305.
[47] F. Weigend, Accurate Coulomb-fitting basis sets for H to Rn, Phys. Chem. Chem. Phys. 8 (2006) 1057–1065.
[48] A.D. Becke, Density-functional thermochemistry. III. The role of exact exchange, J. Chem. Phys. 98 (1993) 5648–5652.
[49] C. Lee, W. Yang, R.G. Parr, Development of the Colle-Salvetti correlation-energy formula into a functional of the electron density, Phys. Rev. B 37 (1988) 785–789.
[50] P.J. Stephens, F.J. Devlin, C.F. Chabalowski, M.J. Frisch, Ab initio calculation of vibrational absorption and circular dichroism spectra using density functional force fields, J. Phys. Chem. 98 (1994) 11623–11627.
[51] T.H. Dunning Jr, Gaussian basis sets for use in correlated molecular calculations. I. The atoms boron through neon and hydrogen, J. Chem. Phys. 90 (1989) 1007–1023.
[52] R.L. Martin, P.J. Hay, L.R. Pratt, Hydrolysis of ferric ion in water and conformational equilibrium, J. Phys. Chem. A 102 (1998) 3565–3573.
[53] A. Poater, E. Pump, S.V.C. Vummaleti, L. Cavallo, The right computational recipe for olefin metathesis with Ru-based catalysts: the whole mechanism of ring-closing olefin metathesis, J. Chem. Theory Comput. 10 (2014) 4442–4448.
[54] S. Manzini, A. Poater, D.J. Nelson, L. Cavallo, A.M.Z. Slawin, S.P. Nolan, Insights into the decomposition of olefin metathesis Pre-catalysts, Angew. Chem. Int. Ed. 53 (2014) 8995–8999.
[55] Y. Minenkov, E. Chermak, L. Cavallo, Troubles in the systematic prediction of transition metal thermochemistry with contemporary out-of-the-box methods, J. Chem. Theory Comput. 12 (2016) 1542–1560.
[56] A.V. Marenich, C.J. Cramer, D.G. Truhlar, Universal solvation model based on solute electron density and on a continuum model of the solvent defined by the bulk dielectric constant and atomic surface tensions, J. Phys. Chem. B 113 (2009) 6378–6396.
[57] S. Sadjadi, M. Atai, Ternary hybrid system of halloysite nanotubes, polyacrylamides and cyclodextrin: an efficient support for immobilization of Pd nanoparticles for catalyzing coupling reaction, Appl. Clay. Sci. 153 (2018) 78–89.
[58] F. Shahangi, A. Najafi Chermahini, M. Saraji, Dehydration of fructose and glucose to 5-hydroxymethylfurfural over Al-KCC-1 silica, J. Energy Chem. 27 (2018) 769–780.
[59] J. Najafi Sarpiri, A. Najafi Chermahini, M. Saraji, A. Shahvar, Dehydration of carbohydrates into 5-hydroxymethylfurfural over vanadyl pyrophosphate catalysts, Renew. Energy 164 (2021) 11–22.
[60] S. Kozuch, K. Shaik, How to conceptualize catalytic cycles? The energetic span model, Acc. Chem. Res. 44 (2011) 101–110.
[61] E. Solel, N. Tarannam, S. Kozuch, Catalysis: energy is the measure of all things, Chem. Commun. 55 (2019) 5306–5322.
[62] A. Gómez-Suárez, Y. Oonishi, A.R. Martin, S.V.C. Vummaleti, D.J. Nelson, D. B. Cordes, A.M.Z. Slawin, L. Cavallo, S.P. Nolan, A. Poater, On the Mechanism of the Digold(I)-Hydroxide-Catalysed Hydrophenoxylation of Alkynes, Chem. Eur. J. 22 (2016) 1125–1132.
[63] A. Poater, S.V.C. Vummaleti, E. Pump, L. Cavallo, Comparing Ru and Fe-catalyzed olefin metathesis, Dalton Trans. 43 (2014) 11216–21122.
[64] E.R. Johnson, S. Keinan, P. Mori-Sanchez, J. Contreras-Garcia, A.J. Cohen, W. T. Yang, Revealing noncovalent interactions, J. Am. Chem. Soc. 132 (2010) 6498–6506.
[65] J. Contreras-Garcia, E.R. Johnson, S. Keinan, R. Chaudret, J.P. Piquemal, D. N. Beratan, W.T. Yang, NCIPLOT: a program for plotting noncovalent interaction regions, J. Chem. Theory Comput. 7 (2011) 625–632.
[66] C. Zhu, H. Wang, C. Cai, K. Bi, B. Cai, X. Song, Q. Liu, L. Ma, Tandem conversion of fructose to 2,5-dimethylfuran with the aid of ionic liquids, ACS Sust. Chem. Eng. 7 (2019) 16026–16040.
[67] Y. Román-Leshkov, C.J. Barrett, Z.Y. Liu, J.A. Dumesic, Production of dimethylfuran for liquid fuels from biomass-derived carbohydrates, Nature 447 (2007) 982–985.